ORIGINAL PAPER

Applying Eigenstructure Assignment to Inner-Loop Flight Control Laws for a Multibody Aircraft

Alexander Köthe[1] · Robert Luckner[1]

Abstract

Unmanned aircraft used as high-altitude platform system has been studied in research and industry as alternative technologies to satellites. Regarding actual operation and flight performance of such systems, multibody aircraft seems to be a promising aircraft configuration. In terms of flight dynamics, this aircraft strongly differs from classical rigid-body and flexible aircraft, because a strong interference between flight mechanic and formation modes occurs. For unmanned operation in the stratosphere, flight control laws are required. While control theory generally provides a number of approaches, the specific flight physics characteristics can be only partially considered. This paper addresses a flight control law approach based on a physically exact target model of the multibody aircraft dynamics rather than conventionally considering the system dynamics only. In the target model, hypothetical spring and damping elements at the joints are included into the equations of motion to transfer the configuration of a highly flexible multibody aircraft into one similar to a classical rigid-body aircraft. The differences between both types of aircraft are reflected in the eigenvalues and eigenvectors. Using the eigenstructure assignment, the desired damping and stiffness are established by the inner-loop flight control law. In contrast to other methods, this procedure allows a straightforward control law design for a multibody aircraft based on a physical reference model.

Keywords Flight control theory · Control allocation · Multibody aircraft · Highly flexible aircraft structures

1 Introduction

Aircraft operating as so-called High-Altitude Platform Systems (HAPS) have been considered as a complementary technology to satellites for several years. These aircraft can be used for similar communication and monitoring tasks while operating at a fraction of the cost. Such concepts have been successfully tested. Those include the AeroVironment Helios [13] and, in particular, the Airbus *Zephyr*, with a proven endurance of nearly 624 hours (26 days) [1]. All these HAPS aircraft have a single high-aspect-ratio wing using lightweight construction. In gusty atmosphere, this results in high bending moments and high structural loads, which can lead to overloads. Aircraft accidents, for example observed with Google's *Solara 50* [6] or Facebook's *Aquila* [5], give proof of that fact. Especially in the troposphere,

where the active weather takes place, gust loads occur, which can lead to the destruction of the structure. Besides the general challenges regarding long-endurance operation, specific flight performance characteristics are important for HAPS, among which payload capacity is the most prominent. The Airbus *Zephyr*, for example, provides only a very small payload. Thus, it does not fully comply with the expectations towards future HAPS, a phenomenon typically observed with single-wing configurations.

To overcome the shortcomings of aircraft with wings of extreme high aspect ratio and flexibility, so-called *multibody aircraft* are considered to be an alternative. The concept assumes multiple aircraft with wings of low aspect ratio connected to each other at their wingtips to increase the wingspan. The idea dates back to the German engineer Dr. Vogt [12]. In the United States, shortly after the end of World War II, he experimented with the coupling of manned aircraft. This resulted in a high-aspect-ratio wing for the overall aircraft formation. The range of the formation could be increased correspondingly. The engineer Geoffrey S. Sommer took up Vogt's idea and patented an aircraft configuration consisting of several unmanned aerial vehicles

✉ Alexander Köthe
  alexander.koethe@campus.tu-berlin.de

1 Flight Mechanics, Flight Control and Aeroelasticity, Technische Universität Berlin, Marchstraße 12 - F5, 10587 Berlin, Germany

coupled at their wingtips [16]. A flight mechanical analysis (static and dynamic) and the design of flight control laws is missing in Sommer's patent.

In the internal TU Berlin project *AlphaLink*, the flight mechanic design, the flight dynamic modelling and the flight control laws for a multibody aircraft configuration were established. The fundamental differences between the multibody aircraft and a conventional aircraft that can be considered as rigid or flexible are the following:

1. A high-aspect-ratio wing is achieved through wing tip coupling of several individual aircraft with mechanical joints leading to an aircraft structure with multiple, distributed flight controls along the wingspan.
2. The number of the degrees of freedom is finite (depending on the joint configuration and the number of coupled aircraft), as each individual aircraft is assumed to be rigid.
3. The coupling equations between the aircraft are non-linear, but can be expressed mathematically exact.
4. The *formation modes* that occur due to the mechanical wing tip connection do not have any mechanical stiffness or damping and, hence, their eigenvalue and eigenvector characteristics depend only on the aerodynamics.

These special characteristics have to be considered in the flight control law design. The multibody aircraft is an over-actuated multiple input multiple output system. Control theory provides a number of design methods in the time and frequency domain including linear quadratic regulation, optimization or loop shaping. The challenge for all those methods is the right definition of the design goals and the control law structure. In classical flight control, the design goals as well as the flight control law structure shall be derived from the flight physics. This design philosophy is also desired for the multibody aircraft. This article makes a contribution to an inner-loop control law based on a physically correct target model that modifies the flight dynamics of the unconventional multibody aircraft to become similar to the one of a rigid-body aircraft. It is based on former research carried out in a PhD project on flight mechanics and flight control of multi-body aircraft [9]. For this purpose, hypothetical spring element and damping elements at the joints are introduced in the equation of motion. This converts the very flexible aircraft configuration into a nearly rigid-body aircraft, when a high stiffness is used. The eigenvectors of the theoretical rigid-body aircraft are determined and later on used in an eigenstructure assignment to calculate the inner-loop control law for the very flexible aircraft without any spring and damping elements. With this method, the classical, flight mechanical rigid-body modes and the formation modes are well separated from each other. Hence,

the outer loop has to control the rigid-body motion of the aircraft only [10].

2 Reference Aircraft Design

For the aircraft design that is used as reference in this paper, only the most important key facts are mentioned. The main requirement is the operation of the multibody aircraft as HAPS. The following design requirements, derived in part from the U.S. DARPA[1] *Vulture* program [3], are applied:

– Payload capacity shall be 450 kg and the required payload power is 5 kW.
– The aircraft shall continuously operate for at least one year in the mission altitude.
– The design operation latitude is specified at 40° N/S.
– The single aircraft shall be able to fly to the mission altitude and leave the formation and return to ground on their own.
– The single aircraft shall be designed as rigid aircraft.

Those requirements are achieved by an aircraft design with properties that are listed in Table 1. For the design, a planar wing formation is selected, i.e. a configuration where all individual aircraft have the same pitch angle. Figure 1 shows the design of such an aircraft configuration. The mechanical joint between the single aircraft allows a pitch and roll degree of freedom and hence it transmits all reaction forces and the yaw reaction moment. Because of this and the non-uniform lift distribution, the inner aircraft of the formation have to partially carry the weight of the outer aircraft. This causes reaction forces. Considering the free-body diagram of the single aircraft, those reaction forces are not equal in magnitude at the left and right wing tip and, hence, a rolling moment occurs. This moment is amplified by the non-uniform lift distribution for the single aircraft. The roll moment balance can be achieved by flap deflection. On one wing side, the lift is increased while on the other wing side the lift is decreased. Using this method, the lift distribution is influenced, and the additional flap deflections lead to drag. To overcome such difficulties, the center of gravity is shifted along the wingspan. With this, the lever arms are influenced, and an equilibrium of moments is established. Because the battery of the aircraft is nearly the highest single mass component of the aircraft shifting it is used to change the lateral center of gravity position.

Table 1 Selected parameters for the optimized multibody aircraft with planar wing

Span [m]	210.66				
Aspect ratio [1]	55				
Total mass [kg]	4509				
Total battery mass [kg]	1137				
Altitude [m]	20,000				
Airspeed [m s^{-1}]	33.37				
Horizontal tail area [m^2]	6.05				
Vertical tail area [m^2]	1.45				
Zero drag coefficient [1]	0.008				
Available sun energy per day [GJ/day]	11.12				
Required sun energy per day [GJ/day]	11.12				
Max. engine power [kW]	11.51				
Long. CG position [m]	− 3.74				
Neutral point wing [m]	− 3.26				
Distance wing tail [m]	11.49				
Half span per aircraft [m]	10.53				
	AC1	AC2	AC3	AC4	AC5
Angle of attack [1°]	4.8	4.8	4.8	4.8	4.8
Elevator deflection [1°]	− 3.58	− 6.05	− 6.4	− 6.51	− 6.55
Trim engine power [kW]	5.29	2.04	1.49	1.29	1.22
Lat. CG position [m]	1.69	2.12	1.68	1.05	0.36
Battery shift [m]	6.7	8.39	6.65	4.17	1.42

3 Flight Dynamic Model

The flight dynamics of the multibody aircraft that was designed for operation as a HAPS are now analyzed. The following assumptions are made:

1. The multibody aircraft consists of multiple single aircraft, all being individually rigid aircraft. Aeroelasticity of the single aircraft is not considered due to the structural design.
2. The aerodynamic forces are modeled using potential flow theory (vortex lattice method).
3. The engine is ideal. Energy dissipation due to friction is considered but impacts of propeller rotational speed and blade pitch angles are not considered.
4. Thrust force acts in x-direction of the body-fixed axes system without moment about the center of gravity of the single aircraft.
5. There is no gap between the aircraft. It is assumed that there is a seal, which prevents flow from the lower to the upper surface.
6. The joint connections between two single aircraft are considered to be ideal, i.e. without natural friction, damping or spring forces.

3.1 Equations of Motion

The equations of motion are derived using Kane's method [8]. They are formulated as:

$$\tilde{\mathbf{F}}_r + \tilde{\mathbf{F}}_r^{\star} = 0 \quad (r = 1, \ldots, p), \tag{1}$$

where $\tilde{\mathbf{F}}_r$ is the vector of the generalized active forces, $\tilde{\mathbf{F}}_r^{\star}$ is the vector of the generalized inertial forces in the reference frame and p is the number of the generalized speeds. In Eq. 1, the denotation "generalized force" includes inertial and active forces as well as inertial and active moments (translation and rotation) [8]. The generalized inertial force is determined with

$$\tilde{\mathbf{F}}_r^{\star} = -\sum_{j=1}^{l} {}^{N}\mathbf{F}_k^{CG,j} \frac{\partial {}^{N}\mathbf{v}^{CG,j}}{\partial u_r} - \sum_{j=1}^{l} {}^{N}\mathbf{M}_k^{CG,j} \frac{\partial {}^{N}\boldsymbol{\omega}^{B,j}}{\partial u_r}, \tag{2}$$

where ${}^{N}\mathbf{v}^{CG,j}$ is the velocity of the center of gravity (CG) of the jth body in the Newtonian frame, ${}^{N}\boldsymbol{\omega}^{B,j}$ the angular velocity of the body frame about the Newtonian frame of the jth body, u_r are the generalized speeds, and $\mathbf{F}_k$ and $\mathbf{M}_k$ are force and moment of the jth body decomposed as
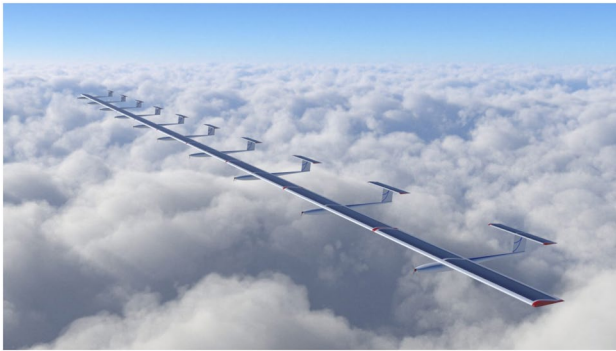
Fig. 1 Illustration of the reference aircraft configuration

Fig. 2 Reaction forces and moments for a joint with pitch and roll degree of freedom between two aircraft

$$^N\mathbf{F}_{\mathrm{k}}^{CG} = m\left(\frac{d\ ^B\mathbf{v}^{CG}}{dt} + ^N\boldsymbol{\omega}^B \times ^B\mathbf{v}^{CG}\right) \quad \text{and} \tag{3}$$
$$^N\mathbf{M}_{\mathrm{k}}^{CG} = \mathbf{I}^N\dot{\omega}^B + ^N\omega^B \times \left(\mathbf{I}\ ^N\omega^B\right),$$

with l representing the number of rigid bodies in the system. The generalized active force is given by

$$\tilde{\mathbf{F}}_{\mathrm{r}} = \sum_{j=1}^{l} {}^N\mathbf{F}_{\mathrm{a}}^{CG,j} \frac{\partial ^N\mathbf{v}^{CG,j}}{\partial u_{\mathrm{r}}} + \sum_{j=1}^{l} {}^N\mathbf{M}_{\mathrm{a}}^{CG,j} \frac{\partial ^N\boldsymbol{\omega}^{B,j}}{\partial u_{\mathrm{r}}}, \tag{4}$$

where $\mathbf{F}_{\mathrm{a}}$ and $\mathbf{M}_{\mathrm{a}}$ are the forces and moments acting at the center of gravity. The coupling within the equations of motion is carried by motion constrains. Figure 2 shows the free-body diagram for the selected joint configuration that allows a pitch and roll motion between the aircraft. At the joints, the nonholonomic motion constraints

$$\begin{pmatrix} ^N\mathbf{v}^{CAB} - ^N\mathbf{v}^{CBA} \end{pmatrix}\mathbf{e}_{\mathrm{x,g}} = 0, \quad \begin{pmatrix} ^N\mathbf{v}^{CAB} - ^N\mathbf{v}^{CBA} \end{pmatrix}\mathbf{e}_{\mathrm{y,g}} = 0,$$
$$\begin{pmatrix} ^N\mathbf{v}^{CBA} - ^N\mathbf{v}^{CAB} \end{pmatrix}\mathbf{e}_{\mathrm{z,g}} = 0, \quad \begin{pmatrix} ^N\boldsymbol{\omega}^A - ^N\boldsymbol{\omega}^B \end{pmatrix}\mathbf{e}_{\mathrm{z,g}} = 0, \tag{5}$$

are valid with $^N\mathbf{v}^{CAB}$ as body-fixed velocity of the point CAB ($^N\mathbf{v}^{CBA}$ of point CBA) in the Newtonian reference frame, $\mathbf{e}$ as unit vector of the Newtonian reference frame and $^N\omega^A$ of aircraft A ($^N\omega^B$ of aircraft B) as angular velocity in the Newtonian reference frame. For this configuration, the non-linear differential equations of motions that describe the dynamic behavior of the multibody aircraft can be expressed by a first-order non-linear differential equation system that consists of

– **12** non-linear first-order differential equations for the rigid-body motion for the first aircraft at which the others shall couple (velocity, position, rotation rates and Euler angles) and
– **5** non-linear first-order differential equations for each coupled aircraft (roll and pitch rate as well as Euler angles).

For the flight dynamic analysis, the navigation differential equations (position and yaw angle for the rigid-body
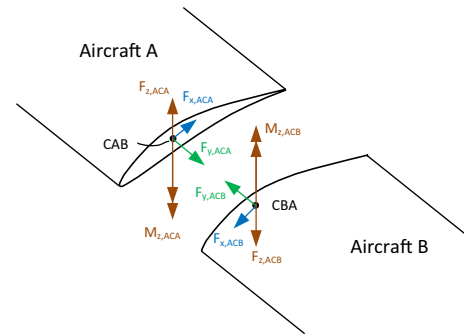
motion as well as yaw angle for every coupled aircraft) can be neglected. This reduces the number of differential equations to eight for the rigid-body motion and to four for every coupled aircraft. In the case of the reference aircraft (ten coupled aircraft), 44 first-order differential equations remain. As external forces, the aerodynamic forces in a body-fixed reference system $\mathbf{R}_{\mathrm{A,b}}$, thrust $\mathbf{T}_{\mathrm{b}}$ in a body-fixed system and weight in the geodetic reference systems $\mathbf{W}_{\mathrm{n}}$ have to considered for every aircraft. The active force at the jth aircraft in the body-fixed reference frame is then determined as

$$^{\mathrm{b}}\mathbf{F}_{\mathrm{a}}^{CG,j} = \mathbf{R}_{\mathrm{A,b,j}} + \mathbf{T}_{\mathrm{b,j}} + \mathbf{T}_{\mathrm{b,n,j}}\,\mathbf{W}_{\mathrm{n,j}}, \tag{6}$$

where $\mathbf{T}_{\mathrm{b,n}}$ is the transformation matrix from the Newtonian/geodetic reference frame (index n) to the body-fixed reference frame. Applying the introduced assumptions, the aerodynamic moment in the body-fixed system $\mathbf{M}_{\mathrm{A,b}}$ is the only generalized external moment. Hence, the active moment of the jth aircraft in the body-fixed reference frame is

$$^{\mathrm{b}}\mathbf{M}_{\mathrm{a}}^{CG,j} = \mathbf{M}_{\mathrm{A,b,j}}. \tag{7}$$

The aerodynamic forces and moments are calculated using the vortex lattice method for every aircraft [7]. The introduced formulations are sufficient to describe the flight dynamic model of the rigid-body aircraft.

As described in the introduction, the later used eigenstructure assignment requires a flight dynamic model with hypothetical spring and damping elements at joints. Compared to flexible aircraft, these elements provide the very flexible multibody aircraft with structural stiffness and damping. For every joint connecting an aircraft j with an aircraft $j+1$, the effect of the spring on the roll motion (bending) is modeled using the moment $M_{\mathrm{s},\Phi}$ and the effect on the pitch motion (torsion) using the moment $M_{\mathrm{s},\Theta}$ with

$$\begin{aligned} M_{\mathrm{s},\Phi} &= k_{\Phi}\big(\Phi_j - \Phi_{j+1}\big) \\ M_{\mathrm{s},\Theta} &= k_{\Theta}\big(\Theta_j - \Theta_{j+1}\big) \end{aligned}, \tag{8}$$

where k_Φ and k_Θ are spring constants and Θ and Φ are the pitch and bank angle. The same procedure is carried out for the damping moments using the roll rate p and the pitch rate q. The damping moments for the rolling and pitching moment are

$$
\begin{aligned}
M_{\mathrm{d},\Phi} &= d_\Phi\big(p_i - p_{i+1}\big) \\
M_{\mathrm{d},\Theta} &= d_\Theta\big(q_i - q_{i+1}\big)
\end{aligned}. \tag{9}
$$

These moments act in the Newtonian reference frame and are added to the active moments of Eq. 7 with

$$
{}^{\mathrm{b}}\mathbf{M}_{\mathrm{a}}^{\mathrm{CG,j}} = \mathbf{M}_{\mathrm{A,b,j}} + \dots
$$
$$
\mathbf{T}_{\mathrm{b,n,j}} \begin{bmatrix} M_{\mathrm{d},\Phi,j-1} + M_{\mathrm{s},\Phi,j-1} - M_{\mathrm{d},\Phi,j} - M_{\mathrm{s},\Phi,j} \\ M_{\mathrm{d},\Theta,j-1} + M_{\mathrm{s},\Theta,j-1} - M_{\mathrm{d},\Theta,j} - M_{\mathrm{s},\Theta,j} \\ 0 \end{bmatrix} \tag{10}
$$

where $\mathbf{T}_{\mathrm{b,n}}$ is the transformation matrix from the Newtonian/geodetic reference frame (index n) to the body-fixed reference frame. Eq. 10 represents a general formulation for the case that the considered aircraft is coupled with other aircraft on the left and right wing tip. If there is only a one-sided coupling, only one damping and spring moment for pitch and roll motion must be considered.

3.2 Non-linear Simulation Model and Linearization

The non-linear equations of motion, which include the computation of the aerodynamics with the vortex lattice method, and the kinematic relations must be solved numerically. This leads to a system

$$
\begin{aligned}
\dot{\mathbf{x}} &= \mathbf{f}(\mathbf{x}, \mathbf{u}, \mathbf{z}) \\
\mathbf{y} &= \mathbf{g}(\mathbf{x}, \mathbf{u}, \mathbf{z})
\end{aligned} \tag{11}
$$

with $\mathbf{x}$ as state vector, $\mathbf{u}$ as input vector, $\mathbf{z}$ as disturbance vector and $\mathbf{y}$ as output vector. The non-linear function $\mathbf{f}(\mathbf{x}, \mathbf{u}, \mathbf{z})$ represents the dynamic behavior, while the function $\mathbf{g}(\mathbf{x}, \mathbf{u}, \mathbf{z})$ maps state, input and disturbance variables to desired outputs. All elements are integrated into a Simulink model. The reference design of ten aircraft has 44 integrators (neglecting position of the formation and yaw angle of the coupled aircraft). The fifth aircraft is selected as reference aircraft. Thus, the state vector comprises the following 44 states:

$$
\begin{aligned}
\mathbf{x} = \big[& u_{\mathrm{kf,AC5}}, v_{\mathrm{kf,AC5}}, w_{\mathrm{kf,AC5}},\ p_{\mathrm{kf,AC5}}, q_{\mathrm{kf,AC5}}, \dots \\
& r_{\mathrm{kf,AC5}},\ \Theta_{\mathrm{AC5}},\ \Phi_{\mathrm{AC5}},\ \mathbf{x}_{\mathrm{AC1}}, \mathbf{x}_{\mathrm{AC2}}, \mathbf{x}_{\mathrm{AC3}}, \dots \\
& \mathbf{x}_{\mathrm{AC4}}, \mathbf{x}_{\mathrm{AC6}}, \mathbf{x}_{\mathrm{AC7}}, \mathbf{x}_{\mathrm{AC8}}, \mathbf{x}_{\mathrm{AC9}}, \mathbf{x}_{\mathrm{AC10}} \big]^T
\end{aligned}
$$
$$
\text{with}\quad \mathbf{x}_{\mathrm{AC}i} = \begin{bmatrix} q_{\mathrm{AC}i} \\ \Theta_{\mathrm{AC}i} \\ p_{\mathrm{AC}i} \\ \Phi_{\mathrm{AC}i} \end{bmatrix}^T \quad \text{and} \quad i = 1, \dots 10. \tag{12}
$$

with $u_{\mathrm{kf,AC5}}$, $v_{\mathrm{kf,AC5}}$ and $w_{\mathrm{kf,AC5}}$ as flight path velocities in the body-fixed reference frame, p as roll rate, q as pitch rate, r as yaw rate, Φ as bank angle and Θ as pitch angle. In case of the reference aircraft, the classical flight mechanics states shall be used, where the three generalized speed components are replaced by the airspeed $\mathbf{V}_{\mathrm{A}}$, angle of attack α and sideslip angle β. The relations are given in [2]. It follows an output vector with

$$
\begin{aligned}
\mathbf{y} = \big[& q_{\mathrm{AC5}}, \alpha_{\mathrm{AC5}}, V_{\mathrm{AC5}}, \Theta_{\mathrm{AC5}}, r_{\mathrm{AC5}}, \beta_{\mathrm{AC5}}, p_{\mathrm{AC5}}, \dots \\
& \Phi_{\mathrm{AC5}}, \mathbf{y}_{\mathrm{AC1}}, \mathbf{y}_{\mathrm{AC2}}, \mathbf{y}_{\mathrm{AC3}}, \mathbf{y}_{\mathrm{AC4}}, \dots \\
& \mathbf{y}_{\mathrm{AC6}}, \mathbf{y}_{\mathrm{AC7}}, \mathbf{y}_{\mathrm{AC8}}, \mathbf{y}_{\mathrm{AC9}}, \mathbf{y}_{\mathrm{AC10}} \big]^T
\end{aligned}
$$
$$
\text{with}\quad \mathbf{y}_{\mathrm{AC}i} = \begin{bmatrix} q_{\mathrm{AC}i} \\ \Theta_{\mathrm{AC}i} \\ p_{\mathrm{AC}i} \\ \Phi_{\mathrm{AC}i} \end{bmatrix}^T \quad \text{and} \quad i = 1, \dots 10. \tag{13}
$$

The elevator deflection η, the left ξ_{left} and right ξ_{right} aileron deflections, the rudder ζ and the thrust F of every aircraft are used as input variables. In summary, 50 input variables are available. The wind is considered as disturbance. It is assumed that a vertical and horizontal wind component can act at each aircraft. This leads to 20 disturbance variables.

To investigate the dynamic behavior, the non-linear model is linearized with MATLAB using numerical perturbation. The state-space equation

$$
\begin{aligned}
\dot{\mathbf{x}}(t) &= \mathbf{A}\,\mathbf{x}(t) + \mathbf{B}\,\mathbf{u}(t) + \mathbf{E}\,\mathbf{z}(t), \\
\mathbf{y}(t) &= \mathbf{C}\mathbf{x}(t) + \mathbf{D}\,\mathbf{u}(t) + \mathbf{F}\,\mathbf{z}(t)
\end{aligned} \tag{14}
$$

follows, representing a system of linear first-order differential equations with $\mathbf{A}$ as system matrix, $\mathbf{B}$ as input matrix, $\mathbf{E}$ as disturbance matrix, $\mathbf{C}$ as output matrix, $\mathbf{D}$ as feedforward matrix and $\mathbf{F}$ as feedforward disturbance matrix [11].

4 Flight Dynamic Analysis

The differences in the flight dynamics are now investigated for the uncontrolled (passive) multibody aircraft with (i) joints that have hypothetical pitch and roll spring elements and (ii) joints with free motion in the final configuration. For the first case, the relation between the spring constant k_Θ and the spring constant k_Φ is used with

$$
k_\Theta = \frac{1}{2.6}\,k_\Phi, \tag{15}
$$

which is similar to the relation between shear modulus G and Young's modulus E for isotropic materials [14]. To establish a rigid-body aircraft configuration, a very high roll stiffness of $k_\Phi = 200\ \mathrm{GNm\ rad^{-1}}$ is used.

Fig. 3 Eigenvalues in the complex plane for a roll stiffness of $k_\Phi = 200$ GNm rad^{-1} (Kinds of motion: *RM* roll mode, *PM* pitch motion, *RYM* roll-yaw motion, *SP* spiral mode, *PH* phugoid)
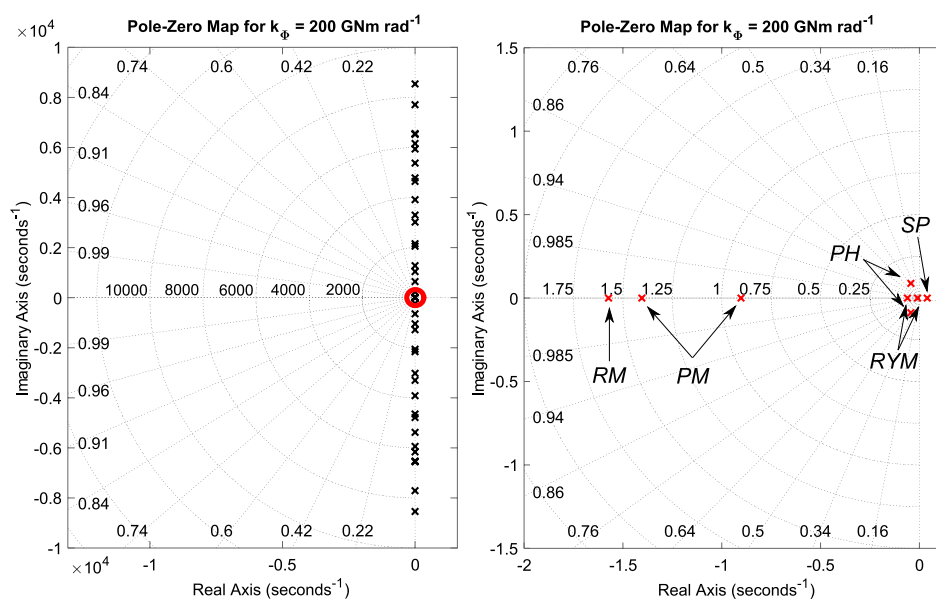
4.1 Artificial Model for Multibody Aircraft Dynamic

The resulting eigenvalues of the linearized state-space system with high stiffness are shown in Fig. 3. The low-frequency eigenvalues belong to the rigid-body flight dynamics and the other ones to the formation modes. The mode identification is carried out with eigenvectors. In the case of the rigid-body modes, the additional coupling degrees of freedom (pitch angle, bank angle, pitch rate and roll rate) have the same phase and magnitude like the reference aircraft. The high-frequency formation shows different phase angles and magnitudes in the entries of the eigenvector. The resulting form of the multibody aircraft formation corresponds to a flexible aircraft structure. Fig. 4 shows the mode shapes of the formation modes with the lowest frequency. Due to the large frequency difference between rigid-body modes and formation modes, a clear separation is possible.

4.2 Multibody Aircraft Dynamic (without spring elements)

Figure 5 shows the eigenvalues of a linearized system with no spring (second case) and, in addition, the identified rigid-body modes of the reference case ($k_\Phi = 200$ GNm rad^{-1}). The rigid-body modes are identified with the help of the eigenvectors. The pitch mode, phugoid and spiral eigenvalues can be detected, while an identification of the roll mode and the Dutch roll is not unequivocal possible. Eigenvalues of formation modes and rigid-body modes are close together.

In contrast to the reference case, the system with no spring elements has eight complex conjugate eigenvalues (four modes) on the right-hand side. The interference between rigid-body modes and formation modes also becomes clear in simulation studies. Using the same inputs that lead to a roll maneuver, the bank angle response is illustrated in Fig. 6 a for a formation with multibody dynamics with hypothetical springs (target model) and in Fig. 6 b without spring. While in the case with spring elements all bank angles have the same magnitude, differences occur in the case without spring and a roll maneuver seems to be impossible.

5 Inner-Loop Flight Control Law Design

The flight dynamic investigation showed that the very flexible multibody aircraft has some unstable poles and an interference between formation modes and rigid-body modes occurs. This behavior was not observed in the case with spring elements and high stiffness. In the control law design, the mechanical stiffness (as well as damping) between the aircraft is established by an inner loop designed with eigenstructure assignment. The desired eigenvalues result from the target model with hypothetical spring elements and damper. Before applying the actual design method, another issue has to be addressed. The number of available inputs is higher than the number of outputs. Such a system is called *over-actuated* [4]. As the eigenstructure assignment can only deal with the same number of inputs and entries to be modified in the eigenvector, the control allocation method has to be applied.
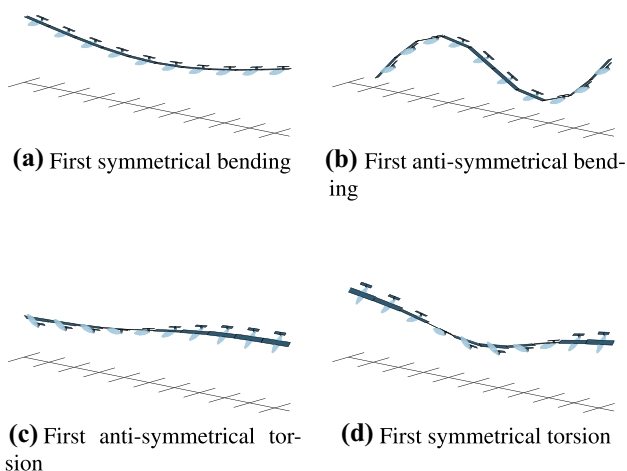
(a) First symmetrical bending

(b) First anti-symmetrical bending

(c) First anti-symmetrical torsion

(d) First symmetrical torsion

Fig. 4 Selected eigenvectors of the formation modes for every kind of motion and a for a roll stiffness of $k_\Phi = 200$ GNm rad^{-1}
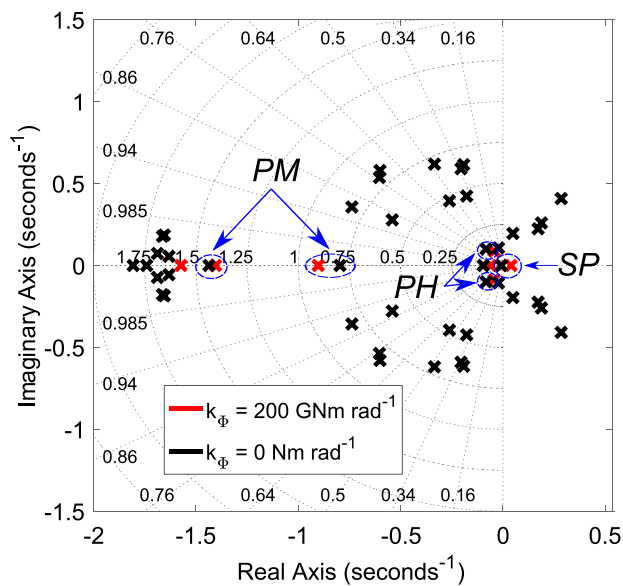

Fig. 5 Eigenvalues for the joint without spring elements and rigid-body eigenvalues of the reference case with a spring stiffness of $k_\Phi = 200$ GNm rad^{-1}

5.1 Control Allocation

In Sect. 3 it was explained that a formation of ten aircraft with joints that do not transmit rolling and pitching moments has 24 degrees of freedom (3 translational degrees of freedom and 21 rotational degrees of freedom). Every translational degree of freedom is affected by a force while a rotational movement is caused by a moment. Thrust as well as aerodynamic surfaces lead to forces and
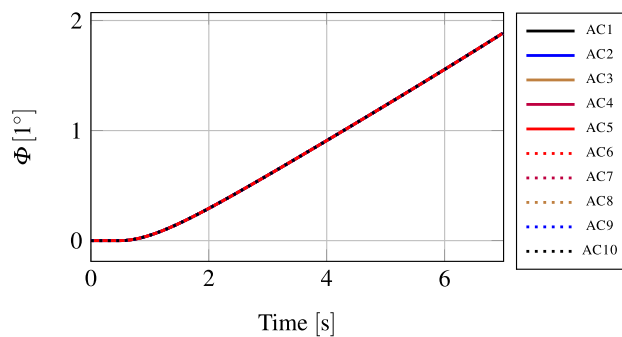
(a) Multibody aircraft dynamic with hypothetical springs
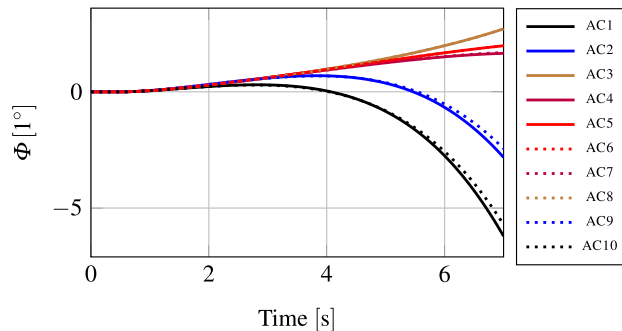
(b) Multibody aircraft dynamic without springs

Fig. 6 Non-linear step response for a roll maneuver

moments. In total, the multibody aircraft has 50 inputs (cf. Sect. 3.2). That means that there are more inputs available than required to influence the degrees of freedom. Such over-actuated systems are handled using control allocation. The main idea of aircraft control allocation is as follows. The control design is not carried out by directly using the aerodynamic surfaces or thrust. Rather, inputs of the aircraft are expressed (indirectly) by moments and forces or their equivalent accelerations and rotational accelerations acting on the aircraft. Those inputs are referred to as *virtual* inputs $\mathbf{v} \in \mathbb{R}^n$. The inputs of the aerodynamic surfaces or thrust are denoted as $\mathbf{u} \in \mathbb{R}^m$ with m as number of *real* inputs. To establish a relation between the two types of inputs, a mapping is applied: $\mathbf{B}_a$ transfers the real inputs to the virtual ones by [4]

$$\mathbf{v} = \mathbf{B}_a \mathbf{u} \quad \text{with} \quad \mathbf{B}_a \in \mathbb{R}^{n \times m}. \tag{16}$$

The control law design is carried out using the virtual inputs.

In case of the multibody aircraft, the derivatives of the generalized speeds (acceleration and rotational acceleration) are used as virtual inputs because they are equivalent to forces and moments. The derivative of the state vector (cf. Eq. 12) contains those 24 derivatives of the generalized speeds. Considering Eq. 14, the mapping matrix $\mathbf{B}_a$

is part of the matrix **B**. Using this allocation, 24 virtual inputs are available for 24 degrees of freedom.

The control law design is carried out using the virtual inputs. By applying the transformation of Eq. 16 to the state-space system of Eq. 14 (without disturbances),

$$
\begin{aligned}
\mathbf{x} &= \mathbf{A}\,\mathbf{x} + \tilde{\mathbf{B}}\,\mathbf{v} \\
\mathbf{y} &= \mathbf{C}\,\mathbf{x} + \tilde{\mathbf{D}}\,\mathbf{v}
\end{aligned}
\tag{17}
$$

follows as new state-space system for the eigenstructure assignment. After the control law design, the inverse matrix mapping the virtual inputs to the real inputs has to be calculated by

$$
\mathbf{u} = \mathbf{P}\,\mathbf{v}.
\tag{18}
$$

Control allocation is thus solving Eq. 16 for **u** [4]. Because $m > n$, the inverse of $\mathbf{B}_a$ does not exist and hence the solution of **P** is not trivial. There are two types of methods to solve the problem: on-line and off-line solutions. So-called on-line solutions are calculating the allocation from the virtual inputs to the real control inputs in real time, while off-line solutions are pre-computed. For the multibody aircraft, the off-line solution is used and described within Sect. 5.4. The block diagram for the control law is shown in Fig. 7.

5.2 Eigenstructure Assignment for the Inner-Loop Control Law

The application of the eigenstructure assignment requires controllability [11]. This condition is fulfilled for the system. The desired eigenvalues are taken from the model with a roll stiffness of $k_\Phi = 200\ \mathrm{GNm\ rad^{-1}}$. To establish damping, a value of $12.8\ 10^6\ \frac{\mathrm{kg\ m^2}}{\mathrm{s}}$ is used for both the pitch d_Θ and roll damping d_Φ coefficient. This leads to nearly rigid-body aircraft with well separated and well damped formation modes. The eigenvalues still have to be modified. Due to the high stiffness, the resulting frequencies of the formation modes are very high. It is known from classical flight control theory that a high desired frequency leads to high gains caused by high aerodynamic surface deflections or thrust [2]. Hence, the frequencies of the formation modes have to be reduced. Since every eigenvalue belongs to a certain eigenvector, the frequency reduction cannot be conducted in an arbitrary way. Therefore, the real and imaginary parts of the eigenvalues are changed using the same relation. The flight mechanics modes (eigenvalues and eigenvectors) should be maintained with the exception of the unstable spiral mode. This eigenvalue is shifted to $\lambda_{\mathrm{SP}} = -0.01$. Hence, the roll mode with $\lambda_{\mathrm{RM}} = -1.57$ is the eigenvalue with the highest magnitude. The formation mode with the lowest frequency should have an undamped frequency (magnitude of the eigenvalue) that is five times higher than the roll mode. This leads to a
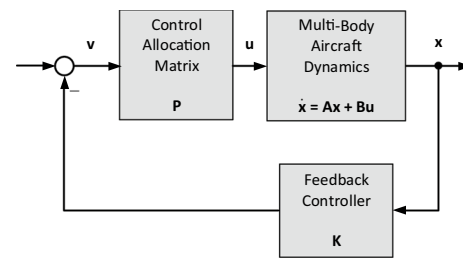

Fig. 7 Control law structure for the design of the inner loops with virtual inputs

desired frequency for the first formation mode (*FOM*) with $\omega_{0,\mathrm{1st\ FOM}} = 8\ \frac{\mathrm{rad}}{\mathrm{s}}$. The differences in the natural frequencies of the formation modes are selected using $\Delta\omega_{0,\mathrm{FOM}} = 1\ \frac{\mathrm{rad}}{\mathrm{s}}$. Thus, the highest natural frequency of the last formation mode is $\omega_{0,\mathrm{16th\ FOM}} = 24\ \frac{\mathrm{rad}}{\mathrm{s}}$. Using this selection, a separation of formation modes and flight mechanics modes is achieved and the desired eigenvectors and eigenvalues for the eigenstructure assignment are selected.

The origin of the eigenstructure assignment is the eigenvalue equation

$$
(\mathbf{A} - \lambda_i \mathbf{I})\mathbf{X}_i = \mathbf{0}
\tag{19}
$$

with **A** as dynamic matrix of the state-space system, λ_i as eigenvalue and $\mathbf{X}_i$ as corresponding eigenvector. According to Fig. 7, the control law for the state feedback is defined with

$$
\mathbf{v} = -\mathbf{K}\,\mathbf{x}.
\tag{20}
$$

Linking Eqs. 19, 20 and the state-space differential equation of Eq. 17 leads to

$$
(\mathbf{A} - \lambda_i \mathbf{I})\mathbf{X}_i = \tilde{\mathbf{B}}\,\mathbf{K}\,\mathbf{X}_i.
\tag{21}
$$

The product of controller and eigenvector is substituted by

$$
\mathbf{r}_i = \mathbf{K}\,\mathbf{X}_i
\tag{22}
$$

and inserted into Eq. 21. After a rearrangement, the result is transformed into matrix notation with

$$
\begin{bmatrix} \mathbf{A} - \lambda_i \mathbf{I} & \tilde{\mathbf{B}} \end{bmatrix}
\begin{bmatrix} \mathbf{X}_i \\ -\mathbf{r}_i \end{bmatrix} = \mathbf{0}.
\tag{23}
$$

The eigenvalue $\mathbf{X}_i$ has 44 elements, but only 24 control inputs are available. This is not an issue, as no input can directly influence the entries of the Euler angles in the eigenvector. Hence, a reduced eigenvector $\tilde{\mathbf{X}}$ is used that contains only the pitch and roll rates of every aircraft (20 elements) as well as the yaw rate, airspeed, angle of attack and sideslip angle of the formation. In sum, the reduced eigenvector has 24 elements, which is equivalent to the number of

virtual inputs. A mapping matrix $\mathbf{M}$ is used to express the full eigenvector as reduced eigenvector by

$$\tilde{\mathbf{X}} = \mathbf{M}\,\mathbf{X} \quad \text{with} \quad \mathbf{M} \in \mathbb{R}^{24 \times 44} . \tag{24}$$

This relation is inserted into Eq. 23, which yields

$$\underbrace{\begin{bmatrix} \mathbf{A} - \lambda_i \mathbf{I} & \tilde{\mathbf{B}} \\ \mathbf{M} & \mathbf{0} \end{bmatrix} \begin{bmatrix} \mathbf{X}_i \\ -\mathbf{r}_i \end{bmatrix}}_{\mathbf{b}_i} = \begin{bmatrix} \mathbf{0} \\ \tilde{\mathbf{X}}_i \end{bmatrix} . \tag{25}$$

Eq. 25 is now solved for $\mathbf{b}_i$ with

$$\mathbf{b}_i = \begin{bmatrix} \mathbf{A} - \lambda_i \mathbf{I} & \tilde{\mathbf{B}} \\ \mathbf{M} & \mathbf{0} \end{bmatrix}^{-1} \begin{bmatrix} \mathbf{0} \\ \tilde{\mathbf{X}}_i \end{bmatrix} . \tag{26}$$

This procedure can be applied to every eigenvalue and the corresponding eigenvalue. Every solution $\mathbf{b}_i$ comprises the vectors $\mathbf{X}_i$ and $\mathbf{r}_i$. The use of Eq. 22 and all $n = 44$ solutions for $\mathbf{b}_i$ leads to

$$\underbrace{\begin{bmatrix} \mathbf{r}_1 & \mathbf{r}_2 & \dots & \mathbf{r}_n \end{bmatrix}}_{\mathbf{R}} = \mathbf{K} \underbrace{\begin{bmatrix} \mathbf{X}_1 & \mathbf{X}_2 & \dots & \mathbf{X}_n \end{bmatrix}}_{\mathbf{X}} \tag{27}$$

that is used to compute the gains of the control law with

$$\mathbf{K} = \mathbf{R}\,\mathbf{X}^{-1} . \tag{28}$$

5.3 Design Results

After selecting the desired eigenvalues and eigenvectors, the methodology of eigenstructure assignment is applied to the linearized state-space system of the multibody aircraft. Eigenvalues of the modified flight dynamics are shown in Fig. 8. The eigenvalues meet the desired values and the system is nominally stable and the flight mechanics modes and the formation modes are separated from each other.

5.4 Solving the Control Allocation Problem

So far, the feedback controller was designed using virtual inputs. These virtual inputs have to be transferred to the real inputs using Eq. 18. A frequently used solution is the Moore-Pensorse pseudo-inverse [4]. This pseudo-inverse reduces the 2-norm of the control vector $\|\mathbf{u}\|_2$. It arises from

$$\mathbf{u} = \underbrace{\mathbf{B}_a^T \left[\mathbf{B}_a\,\mathbf{B}_a^T \right]^{-1}}_{\mathbf{P}} \mathbf{v} \tag{29}$$

as a solution of the control allocation with $\mathbf{P}$ as pseudo-inverse [4]. Instead of minimizing $\mathbf{u}^T\,\mathbf{u}$, a weighting matrix can be used to take different control efforts into account. The use of a diagonal matrix with

$$\mathbf{W} = \mathrm{diag}\left(\frac{1}{|u_{\max}|} \right) \quad \text{with} \quad \mathbf{W} \in \mathbb{R}^{n \times n} \tag{30}$$

reduces the $\mathbf{u}^T\,\mathbf{W}^T\,\mathbf{u}\,\mathbf{W}$. For the aerodynamic surfaces, a maximum value of 30° and for the engine power of 11.51 kW is used. The solution of the control allocation problem is now given with

$$\mathbf{u} = \underbrace{\mathbf{W}^{-1}\mathbf{B}_a^T \left[\mathbf{B}_a\,\mathbf{W}^{-1}\,\mathbf{B}_a^T \right]^{-1}}_{\mathbf{P}} \mathbf{v}. \tag{31}$$

Based on the introduced virtual inputs, the subsequent outer loops shall command a pitch and roll rate derivative for the complete formation to influence the rigid-body dynamics. This can be established using a generalized pitch rate derivative $\dot{q}_{\mathrm{gen,\,input}}$ for all pitch rate derivatives in the virtual control input $\mathbf{v}$. This is expressed by

$$\dot{q}_{\mathrm{kf,\,AC}i,\,\mathrm{input}} = \dot{q}_{\mathrm{gen,\,input}} - \cdots \\ \dot{q}_{\mathrm{kf,\,AC}i,\,\mathrm{input,\,IL}} \quad \forall\, i \in [1, 10] . \tag{32}$$

with $\dot{q}_{\mathrm{kf,\,AC}i,\,\mathrm{input}}$ as virtual pitch rate derivative input in the control allocation matrix and $\dot{q}_{\mathrm{kf,\,AC}i,\,\mathrm{input,\,IL}}$ as pitch rate derivative of the inner loops. The same approach is used for the bank angle control law. Now, a generalized roll rate derivative $\dot{p}_{\mathrm{gen,\,input}}$ is used as a common input for all virtual inputs of the roll rate derivatives with

$$\dot{p}_{\mathrm{kf,\,AC}i,\,\mathrm{input}} = \dot{p}_{\mathrm{gen,\,input}} - \cdots \\ \dot{p}_{\mathrm{kf,\,AC}i,\,\mathrm{input,\,IL}} \quad \forall\, i \in [1, 10] . \tag{33}$$

The control allocation problem is solved accordingly and the combination of control law $\mathbf{K}$ and control allocation matrix $\mathbf{P}$ is tested in non-linear simulations. Figure 9 shows a non-linear pitch angle response for a step input in the generalized pitch rate derivative of $0.1°\,\mathrm{s}^{-2}$. Figure 10 shows the bank angle response for a step input in the generalized roll rate derivative of $0.1°\,\mathrm{s}^{-2}$. In contrast to the open-loop results for the multibody aircraft dynamics without spring elements (cf. Fig. 6), the pitch and bank angles for all aircraft are equal. This shows that the inner loop successfully separates the formation modes from the rigid body modes. The missing stiffness at the joints is mimicked by the control law.

6 Conclusion and Outlook

This paper shows an approach for the inner-loop control laws of a multibody aircraft based on an artificial but physically exact target model. A multibody aircraft is a very flexible aircraft configuration that strongly differs from conventional aircraft. The flight dynamics show a strong interference
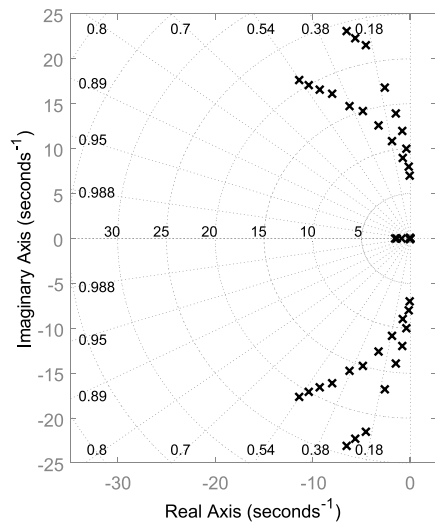
(a) All eigenvalues
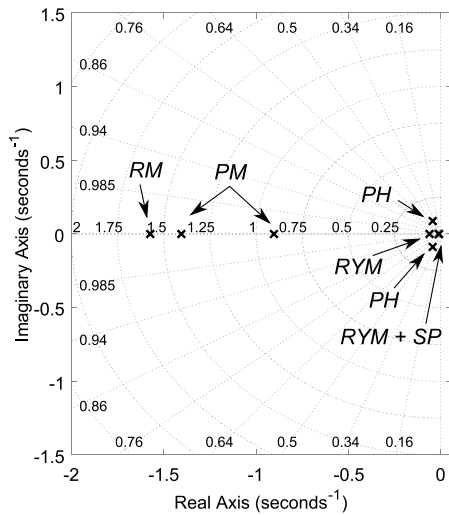
(b) Flight mechanics modes

Fig. 8 Eigenvalues of the multibody aircraft's flight dynamics after applying eigenstructure assignment
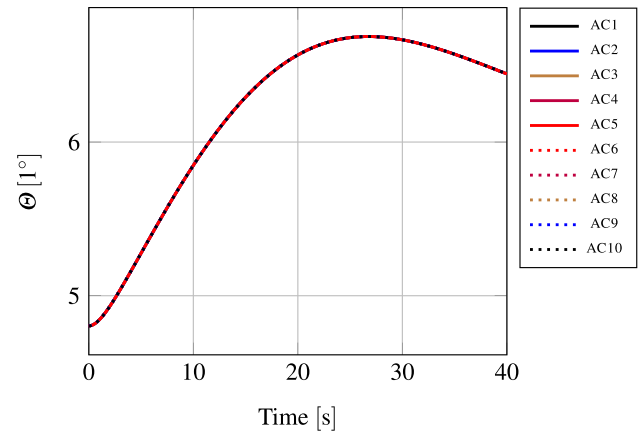

Fig. 9 Non-linear response of all pitch angles for a step input in the generalized pitch rate derivative of $0.1°\,\text{s}^{-2}$

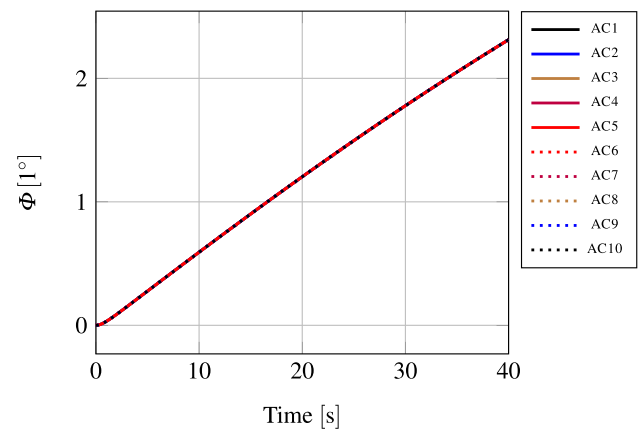**Fig. 10** Non-linear response of all bank angles for a step input in the generalized roll rate derivative of $0.1°\,\text{s}^{-2}$

between classical, flight dynamic rigid-body modes and formation modes that are caused by the joint connection between the aircraft. To separate the modes, a suitable control method is required. This opens the question regarding the right position of the desired eigenvalues and eigenvectors. Using hypothetical spring and damping elements at the joint transforms the highly flexible aircraft into a system similar to a rigid-body aircraft. The resulting eigenvector and scaled eigenvalues stem from an artificial, but physically correctly motivated model and are successfully applied to the design of the inner loops using eigenstructure assignment. A clear definition of the design goals becomes possible, providing an advantage in comparison to other methods like the loop shaping or the linear quadratic regulator.

In further investigations, the proposed method can be used for aircraft with aeroelastic deformations. Using modal transformation, a physically exact target model with high stiffness can be used to define the design goals for inner loops. So far, the non-linear effects of the plant were not considered. Using an eigenstructure assignment with uncertainties could increase the robustness of the inner loops.

References

1. Defence A.: Airbus zephyr solar high altitude pseudo-satellite flies for longer than any other aircraft during its successful maiden flight, https://www.airbus.com/newsroom/press-releases/en/2018/08/Airbus-Zephyr-Solar-High-Altitude-Pseudo-Satellite-flies_for-longer-than-any-other-aircraft.html (2018)
2. Brockhaus, R., Alles, W., Luckner, R.: Flugregelung, vol. 3. Springer, Berlin (2013)
3. Defense Advanced Research Projects Agency.: DARPA bridging the gap powered by ideas. https://apps.dtic.mil/sti/pdfs/ADA510795.pdf (2009)
4. Durham, W., Bordignon, K.A., Beck, R.: Aircraft control allocation. Wiley, Hoboken (2017)
5. Gomez, M.L.: Aviation accident final report, NTSB identification: DCA16CA197
6. Jackmann, C.: Aviation accident final report, NTSB identification: DCA15CA117, National Transportation Safety Board (2015)
7. Katz, J., Plotkin, A.: Low-speed aerodynamics, vol. 13. Cambridge University Press, Cambridge (2001)
8. Kane, T.R., Levinson, D.A.: Dynamics, theory and applications. McGraw Hill, New York (1985)
9. Köthe, A.: Flight Mechanics and flight control for a multibody aircraft: long-endurance operation at high altitudes. Universitätsverlag der TU Berlin, Berlin (2019)
10. Köthe, A., Luckner, R.: Outer-loop control law design with control allocation for a multibody aircraft. EuroGNC, Milan (2019)
11. Levine, W.S.: The control systems handbook: control system advanced methods. CRC Press, Boca Raton (2010)
12. Lockett, B.: Flying aircraft carriers of the USAF: wing tip coupling. Lulu.com, Morrisville (2013)
13. Noll, T.E., Brown, J.M., Perez-Davis, M.E., Ishmael, S.D., Tiffany, G.C., Gaier, M.: Investigation of the helios prototype aircraft mishap, vol. I. ASA Langley Research Center, Virginia (2004)
14. Schnell, W., Gross, D., Hauger, W.: Technische mechanik: band elastostatik. Springer, Berlin (2013)
15. Skogestad, S., Postlethwaite, I.: Multivariable feedback control: analysis and design, vol. 2. Wiley, Hoboken (2007)
16. Sommer, G.S.: Modular articulated-wing aircraft. US Patent 9,387,926 (2016)